




## ORIGINAL ARTICLE

# Boson peak and structural heterogeneity in ternary $\text{SiO}_2\text{-Al}_2\text{O}_3\text{-B}_2\text{O}_3$ glasses

Mariana Fatobene Ando<sup>1</sup> | Sindy Fuhrmann<sup>1,2</sup> | Zhiwen Pan<sup>1</sup> | Bruno Poletto Rodrigues<sup>1</sup> | Tatsuya Mori<sup>3</sup>  | Stefan G. Ebbinghaus<sup>4</sup>  | Katrin Wondraczek<sup>5</sup> | Suguru Kitani<sup>6</sup> | Lothar Wondraczek<sup>1</sup> 

<sup>1</sup>Otto Schott Institute of Materials Research, University of Jena, Jena, Germany

<sup>2</sup>Institute of Glass and Glass Technology, Technical University Bergakademie Freiberg, Freiberg, Germany

<sup>3</sup>Department of Materials Science, University of Tsukuba, Ibaraki, Japan

<sup>4</sup>Institute of Chemistry, Martin Luther University Halle-Wittenberg, Halle, Germany

<sup>5</sup>Leibniz Institute of Photonic Technology, Jena, Germany

<sup>6</sup>Laboratory for Materials and Structures, Tokyo Institute of Technology, Yokohama, Japan

## Correspondence

Lothar Wondraczek, Otto Schott Institute of Materials Research, University of Jena, 07743 Jena, Germany.  
Email: lothar.wondraczek@uni-jena.de

## Funding information

H2020 European Research Council, Grant/Award Number: 681652; Carl Zeiss Foundation

## Abstract

We use low-temperature heat capacity, low-frequency Raman scattering, and THz time domain spectroscopy in order to scale the vibrational density of states and the Boson peak in  $\text{SiO}_2\text{-Al}_2\text{O}_3\text{-B}_2\text{O}_3$  Yb-laser host glasses. When substituting  $\text{B}_2\text{O}_3$  for  $\text{SiO}_2$  at constant  $\text{Al}_2\text{O}_3$  dopant level, we find an optimal value for the ratio of B/Al in terms of mixture stability, at which the excess in the electron donor capability of  $\text{Al}_2\text{O}_3$  (relative to the  $\text{SiO}_2$  backbone) is compensated by the more acidic  $\text{B}_2\text{O}_3$ . At this composition,  $\text{Al}_2\text{O}_3$  plays a mediating role in the structure of aluminoborosilicate glasses, facilitating dissolution of  $\text{Yb}_2\text{O}_3$  and admixture of  $\text{B}_2\text{O}_3$  into the  $\text{SiO}_2$  network.

## KEYWORDS

glass, heterogeneity, optical fiber, silica, Yb-doping

## 1 | INTRODUCTION

Vitreous silica and silica derivatives are benchmark materials for high-power fiber lasers. Depending on operation wavelength, they may incorporate a variety of rare-earth activator species such as Yb or Tm ions. Additions such as  $\text{Al}_2\text{O}_3$  or  $\text{B}_2\text{O}_3$  are used in order to modify the silica backbone towards tailored optical performance (*e.g.*, reducing activator

interactions at maximum activator concentration).<sup>1</sup> Specific formulations are often found in empirical ways, mostly subject to the constraints of high-purity synthesis routes in terms of achievable dopant levels and material homogeneity. More systematic design strategies require an improved understanding of the specific interactions of minor components within the backbone of vitreous silica. Despite several studies made in the  $\text{SiO}_2\text{-Al}_2\text{O}_3\text{-B}_2\text{O}_3$  (SAB) glass system, there are still

This is an open access article under the terms of the Creative Commons Attribution-NonCommercial License, which permits use, distribution and reproduction in any medium, provided the original work is properly cited and is not used for commercial purposes.

© 2021 The Authors. *Journal of the American Ceramic Society* published by Wiley Periodicals LLC on behalf of American Ceramic Society (ACERS)

unanswered questions regarding structure, dynamic features, and mixing of the network-forming cations.<sup>2-4</sup> Due to the experimental difficulties of obtaining homogeneous glasses consisting only of glass-forming oxides,<sup>5-10</sup> network modifiers are frequently added to the base composition, which facilitate conventional melt-quenching of glass samples, but fundamentally change the chemical behavior of the glass system due to their strong interactions with the network-forming oxides.<sup>11</sup> Direct measurements of the intermediate-range structure of glasses remain challenging: the length scales of interest surpass the typical scale of pair distribution analysis, but are still below the capabilities of contemporary analytical imaging methodology. In this report, we consider the effect of B<sub>2</sub>O<sub>3</sub> additions on the intermediate-scale structural heterogeneity in Al<sub>2</sub>O<sub>3</sub>-doped silica as a host material for lasing Yb<sup>3+</sup> centers.

Analyzing the vibrational density of states  $g(\omega)$  (VDoS) and its low-frequency anomalies provides a means for probing structural heterogeneity. Most prominently, the so called “Boson peak” (Bp, an excess in the low-frequency [ $\sim$ THz] VDoS), has gained considerable research interest as a universal feature of glassy materials.<sup>12-17</sup> It can be traced experimentally through optical spectroscopy techniques such as low-frequency Raman scattering<sup>18</sup> and THz time domain spectroscopy (THz-TDS),<sup>19</sup> but also, for example, via low-temperature specific heat capacity measurements.<sup>12</sup> It has been established that the spatial variability of elastic properties plays a central role in defining the Bp.<sup>20</sup> Elastic heterogeneity is intrinsically related to the intermediate range order,<sup>21</sup> therefore, investigations of the low-frequency vibrations and their interaction with acoustic waves provide a suitable method for examining structural features of glasses on such length scales.<sup>12,22</sup>

For the present report, we probed the low-frequency modes of ytterbium-doped ternary aluminoborosilicate glasses through the combined analysis of low-temperature heat capacity, low-frequency Raman scattering, and THz time domain spectroscopy. By this approach, we aim to derive design routes for specific glass formulations which would facilitate cation clustering (or de-clustering) toward controlling the interactions between optically active ion species.

## 2 | EXPERIMENTAL PROCEDURES

### 2.1 | Sample preparation

Ternary [(SiO<sub>2</sub>)<sub>98.4-x</sub> - (B<sub>2</sub>O<sub>3</sub>)<sub>x</sub> - (Al<sub>2</sub>O<sub>3</sub>)<sub>1.5</sub>] glasses, with  $1.25 \leq x \leq 9.35$  were prepared by reactive powder sintering of nanoscale silica.<sup>23-25</sup> All glasses were doped with 0.1 mol% Yb<sub>2</sub>O<sub>3</sub> as a representative optical probe for the precipitation of activator species. The constant Al/Yb ratio of  $\sim 15/1$  was kept for all samples in reference to previous studies which

reported a homogeneous distribution of the ytterbium ions at this ratio.<sup>26-30</sup> The presence of SiCl<sub>4</sub> and hydroxyl groups was determined by wavelength-dispersive electron probe microanalysis (WD-EPMA, also used for verifying the overall chemical composition) and FTIR, respectively. The measured impurity concentrations are less than 0.06 mol% of SiCl<sub>4</sub> and less than 10 ppm of OH. All samples were colorless, except for the one with  $x = 1.40$  whose light-yellow coloration is an indicative of the presence of Yb<sup>2+</sup>. In order to determine the ytterbium oxidation state, photoluminescence excitation and emission spectra (PL) of the synthesized samples were taken with a Horiba-Jobin Yvon Fluorolog FL3-22 spectrofluorometer equipped with double grating excitation and emission monochromators in the wavelength range of 265-1100 nm, using a continuous xenon-arc lamp (450 Watts) as an excitation source. The spectra (see Figure S1) confirm that Ytterbium was present primarily in the form of trivalent ions, and that the concentration of Yb<sup>2+</sup> is low for all samples except for the one with  $x = 1.40$ .

### 2.2 | Material characterization

Physical characterization involved the determination of density (Archimedes method, using dry ethanol as immersion liquid) and refractive index (Metricon, Prism coupler 2010, operating at  $\lambda = 633$  and 1300 nm). Longitudinal and transversal sound wave propagation times were measured with an accuracy of 1 ns by means of piezoelectric transducers (Echometer 1077; Karl Deutsch, operating at frequencies 8-12 MHz) and from the results the elastic moduli were calculated.<sup>31-33</sup> The surface and scratch hardness were investigated through instrumented indentation testing with a nanoindenter (G200; Agilent Inc., operating in continuous stiffness mode), equipped with a three-sided Berkovich diamond tip. Measurement conditions of strain-rate sensitivity and scratch hardness methods are described elsewhere.<sup>34,35</sup>

Raman scattering spectra were collected on a Renishaw Invia micro-Raman spectrometer equipped with a notch filter for collecting spectra at low frequencies. Samples were excited with an Argon laser (gratings: 2400 lines/mm) at an excitation wavelength of 514.5 nm. The signal was collected with a CCD camera in the range from 10 to 1998 cm<sup>-1</sup>, using a 50 $\times$  objective. A constant baseline was subtracted individually and all spectra were normalized by their total area. The low-frequency part of the Raman spectra ( $<200$  cm<sup>-1</sup>) was corrected for air scattering. The measured intensity  $I_{\text{exp}}(\omega_R, T)$  was converted into the reduced intensity by<sup>36</sup>

$$I_{\text{red}}(\omega_R) = \frac{I_{\text{exp}}(\omega_R, T)}{[n(\omega_E, T) + 1] \omega_E}, \quad (1)$$

where  $n(\omega_E, T) = \left[ \exp\left(\frac{\hbar \cdot c \cdot \omega_E}{kT}\right) - 1 \right]^{-1}$  is the Bose–Einstein population factor,  $\omega_R$  is the Raman shift in  $\text{cm}^{-1}$ ;  $c$  is the speed of light in vacuum,  $T$  is the absolute temperature, and  $\hbar$  and  $k$  are the Planck and Boltzmann constants, respectively.

THz time-domain spectroscopy (THz-TDS, RT-10000; Tochigi Nikon Corporation) was conducted in the spectral range of 0.2–4 THz, whereby low-temperature-grown GaAs photoconductive antennas were utilized for both the emitter and detector. The time window of the measured THz time-domain waveforms was 54 ps. To account for the effect of multiple reflections within the samples, the complex transmission coefficient  $t(\omega_{TZ})$  as a function of frequency  $\omega_{TZ}$ , was calculated as follows:

$$t(\omega_{TZ}) = t_{vs} t_{sv} \cdot \frac{\exp(i(n_s - 1)d_s \omega_{TZ}/c)}{1 - r_{sv}(\omega_{TZ})^2 \exp(i2n_s d_s \omega_{TZ}/c)}, \quad (2)$$

where  $t_{ij} = 2n_i / (n_i + n_j)$  and  $r_{ij} = (n_i - n_j) / (n_i + n_j)$  are the complex Fresnel's transmission and reflection coefficients, respectively, at the interface between regions  $i$  and  $j$ ;  $n_i$  is the complex refractive index of the region  $i$  and  $d_s$  is the sample thickness. The subscripts  $v$  and  $s$  represent vacuum and sample, respectively. The extinction coefficient  $k$  (imaginary part of the complex refractive index) was converted to the absorption coefficient  $\alpha = 4\pi\kappa\omega_{TZ}/c$ .

Low-temperature isobaric heat capacity measurements were conducted in a physical property measurement system (PPMS; Quantum Design). Samples were cut and polished to small discs of about 2–3 mm in diameter and 1 mm in thickness, with masses of approximately 15 mg. The heat capacity measurements were done via the relaxation technique, at temperature intervals of 10 K between 300 K and 50 K, 5 K between 50 K and 30 K, 2 K between 30 K and 20 K, and 0.5 K between 20 K and 2 K, applying a logarithmically varying step-size. The VDOS,  $g(\omega_{CP})$ , was extracted from specific heat data using the coherent-potential approximation (CPA),<sup>37–39</sup>

$$C_p(T) \propto \int_0^\infty d\omega_{CP} g(\omega_{CP}) (\omega_{CP}/T^2) \frac{e^{\hbar\omega_{CP}/(k_B T)}}{\left[ e^{\hbar\omega_{CP}/(k_B T)} - 1 \right]^2} \quad (3)$$

where,  $C_p(T)$  is the isobaric specific heat and  $\omega_{CP}$  is the frequency in rad/s. The data fit was done by Tikhonov regularization, using the transversal and longitudinal sound velocities and the Debye cut-off  $k_D = (6\pi^2 N/V)^{1/3}$  for input, with  $N$  and  $V$  being the number of atoms and the volume of the system, respectively.

Infrared reflectance spectra were collected on an attenuated total reflection-Fourier transform infrared spectrometer (ATR-FTIR, Perkin Elmer) across the spectral range of 450–4000  $\text{cm}^{-1}$  with a resolution of 16  $\text{cm}^{-1}$ , averaged over

50 individual scans. Absorption spectra were calculated by Kramers–Kronig transformation,  $\alpha(\nu) = 4\pi\nu k(\nu)$ , where  $\alpha(\nu)$  is the absorption coefficient,  $k(\nu)$  is the imaginary part of the complex refractive index, and  $\nu$  is the infrared frequency.

UV-Vis-NIR absorbance spectra were collected on 1 mm thick samples, polished on both sides, with a double-beam spectrophotometer (CARY 5000; Agilent technologies) over 175–3300 nm spectral region.

Complex impedance measurements were taken with a Novocontrol Alpha-A impedance spectrometer paired with a Novotherm temperature control system. Cylindrical samples with a diameter of 8 mm and thickness of 3 mm were polished on both sides and sputtered with a thin gold film. Measurements were made at temperatures from 250°C to 300°C, with intervals of 10°C and at frequencies from  $10^{-1}$  to 107 Hz using a fixed voltage amplitude of 1 V.

Unless otherwise specified, all measurements were conducted at ambient pressure and temperature.

### 3 | RESULTS

#### 3.1 | Physical characterization

The obtained physical properties of the studied glasses are summarized in Table 1. Density, refractive index, and elastic moduli decrease upon the addition of  $\text{B}_2\text{O}_3$ ; surface and scratch hardness values follow the trend of the bulk modulus.<sup>40</sup> The strain-rate sensitivity is a useful probe of the degree of localization of plastic deformation in glasses, with small values indicating more heterogeneous and “confined” flow events.<sup>39–42</sup> The compositional dependence of the strain-rate sensitivity indicates the presence of two regimes: up to ~4.3 mol%, replacing  $\text{SiO}_2$  by  $\text{B}_2\text{O}_3$  results in higher strain-rate sensitivity, indicating that plastic deformation is more homogeneously distributed across the glass network. Beyond that degree of substitution, no further change is observed for  $m$ . A similar compositional dependence is seen in the ratio of scratch hardness to surface hardness, which remains constant up to ~2.5 mol% substitution, and then slowly decreases.

#### 3.2 | Raman- and Infrared Spectroscopy

The Raman spectra of all samples after area normalization are shown in Figure 1A. The overall spectral shape is quite similar for all glasses. The most notable changes are related to the silica main band (~440  $\text{cm}^{-1}$ ): the observed intensity is reduced between pure  $\text{SiO}_2$  glass and the sample with 1.25 mol%  $\text{B}_2\text{O}_3$ , then remains constant

**TABLE 1** Mass density  $\rho$ , refractive index at 633 nm, Young's modulus  $E$ , bulk modulus  $K$ , Poisson's ratio  $\nu$ , atomic packing density  $C_g$ , strain-rate sensitivity  $m$ , and ratio of scratch to surface hardness  $H_s/H$

Concentration $B_2O_3$ (mol%)	$\rho$ (g/cm <sup>3</sup> )	$n$	$E$ (GPa)	$K$ (GPa)	$\nu$	$C_g$	$m$	$H_s/H$
1.25	2.216 ( $\pm 0.006$ )	1.4613 ( $\pm 0.0001$ )	73.3 ( $\pm 0.9$ )	38.4 ( $\pm 0.5$ )	0.182	0.4584	0.0054	0.61
1.40	2.217 ( $\pm 0.002$ )	1.4618 ( $\pm 0.0001$ )	73.3 ( $\pm 1.5$ )	38.4 ( $\pm 0.8$ )	0.182	0.4586	0.0069	0.62
2.50	2.211 ( $\pm 0.003$ )	1.4608 ( $\pm 0.0001$ )	71.4 ( $\pm 1.0$ )	37.5 ( $\pm 0.5$ )	0.183	0.4592	0.0069	0.62
4.30	2.195 ( $\pm 0.004$ )	1.4602 ( $\pm 0.0002$ )	67.3 ( $\pm 1.1$ )	36.1 ( $\pm 0.6$ )	0.190	0.4585	0.0100	0.58
6.85	2.178 ( $\pm 0.004$ )	1.4595 ( $\pm 0.0001$ )	62.2 ( $\pm 1.0$ )	34.3 ( $\pm 0.6$ )	0.198	0.4588	0.0099	0.57
9.35	2.154 ( $\pm 0.001$ )	1.4588 ( $\pm 0.0004$ )	57.5 ( $\pm 0.6$ )	32.9 ( $\pm 0.3$ )	0.209	0.4571	0.0098	0.56

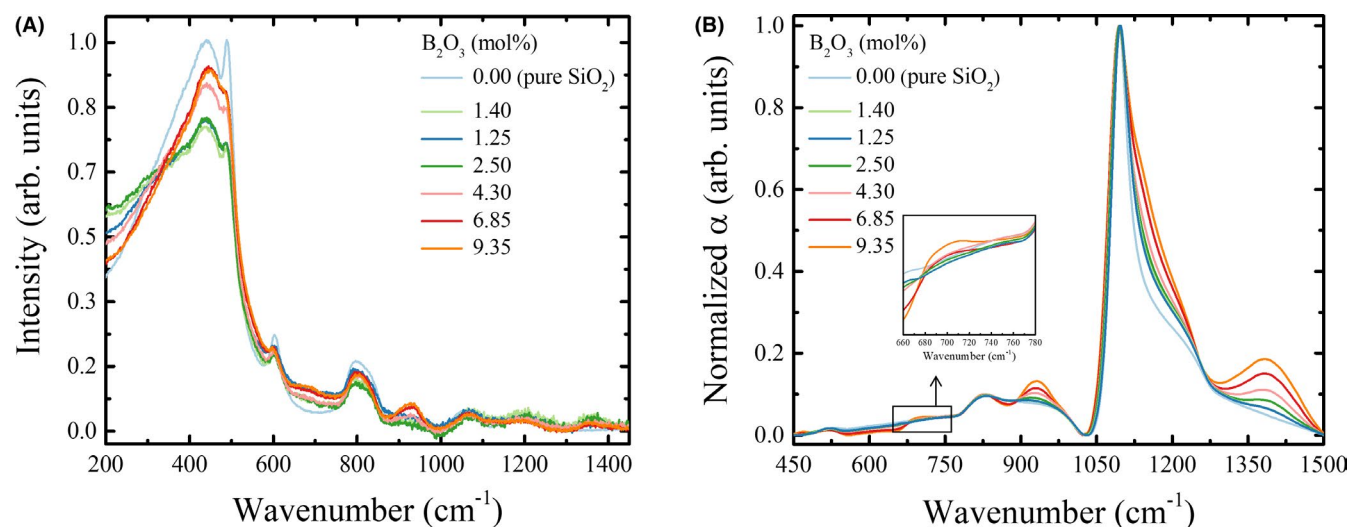


**FIGURE 1** (A) Raman scattering spectra and (B) and normalized absorption coefficient scattering spectra (FTIR) of aluminoborosilicate glasses. Silica glass is shown as a reference [Color figure can be viewed at [wileyonlinelibrary.com](http://wileyonlinelibrary.com)]

up to 2.5 mol% and increases again for higher boron concentrations; the silica defect bands<sup>43</sup> at  $D_1 \sim 490$  cm<sup>-1</sup> and  $D_2 \sim 600$  cm<sup>-1</sup> are similarly affected by the increasing  $B_2O_3$  concentration. The addition of boron oxide also causes the appearance of a broad band at  $\sim 688$  cm<sup>-1</sup>, a strong band located at  $\sim 935$  cm<sup>-1</sup> and a weaker band at  $\sim 1365$  cm<sup>-1</sup>. These bands are assigned to breathing modes of borosilicate rings, Si-O<sup>-</sup> stretching vibrations and isolated [BO<sub>3</sub>] groups, respectively.<sup>44-47</sup>

Figure 1B shows the IR absorption coefficient of the synthesized glasses. In agreement with the Raman scattering data, the IR spectra exhibit similar band shapes among all samples. The spectra are dominated by the characteristic vibrations of vitreous silica. The envelopes between 800-900 cm<sup>-1</sup> and 1050 cm<sup>-1</sup>-1300 cm<sup>-1</sup> correspond to bending and stretching vibrations of the silica network.<sup>48</sup> With the addition of  $B_2O_3$ , two bands emerge at around 932 and 1385 cm<sup>-1</sup>, and a shoulder develops around 1115 cm<sup>-1</sup>. These vibrations are assigned to B-O-Si linkages, BO<sub>3</sub> trigonal groups and Si-O-B vibrations among mixed first-shell neighbors, respectively.<sup>49</sup> Additionally, glasses with  $B_2O_3$

concentrations above 6.85 mol% also develop a weak feature around 700 cm<sup>-1</sup>, which can be attributed to B-O-B bond bending vibrations.<sup>49,50</sup>

### 3.3 | Low-temperature $C_p$ , low-frequency Raman, VDOS and THz-TDS

The reduced low-frequency Raman spectra, excess heat capacity ( $C_p/T^3$ ), VDOS ( $g(\omega)/\omega^2$ ) extracted from specific heat data according to Equation 3, and absorption coefficient from THz-TDS of aluminoborosilicate glasses are shown in Figure 2.

The peak frequencies,  $\omega_{Bp}$ , of Raman,  $C_p$ -VDOS, and THz-TDS are shown in Figure 3. The compositional dependency of the peak position changes for each method used to probe the Bp, reflecting the different natures of the applied stimuli: thermal vibrations ( $C_p$ ) or short- (Raman) and long-wavelength (THz-TDS) electromagnetic waves; regardless, all three change their scaling at 4.3 mol%  $B_2O_3$ . In addition, the low-frequency band intensities inversely follow the  $\omega_{Bp}$ ,



**FIGURE 2** Boson peak in aluminoborosilicate glasses observed by (A) Raman low-frequency scattering, (B) specific heat at low temperature, (C) VDOS normalized over the frequency square as obtained by extraction from specific heat data (CPA) and, (D) THz-TDS [Color figure can be viewed at wileyonlinelibrary.com]

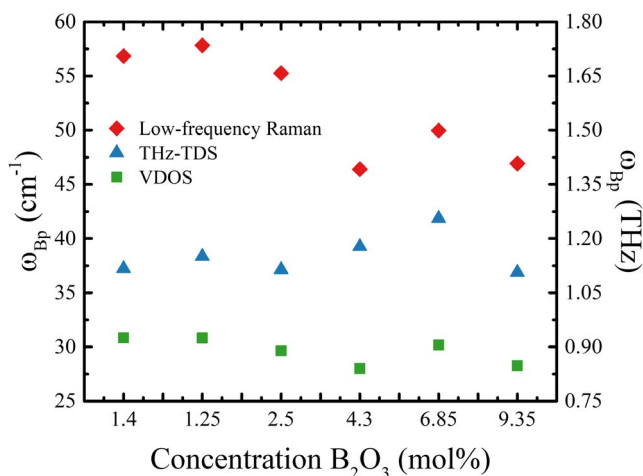
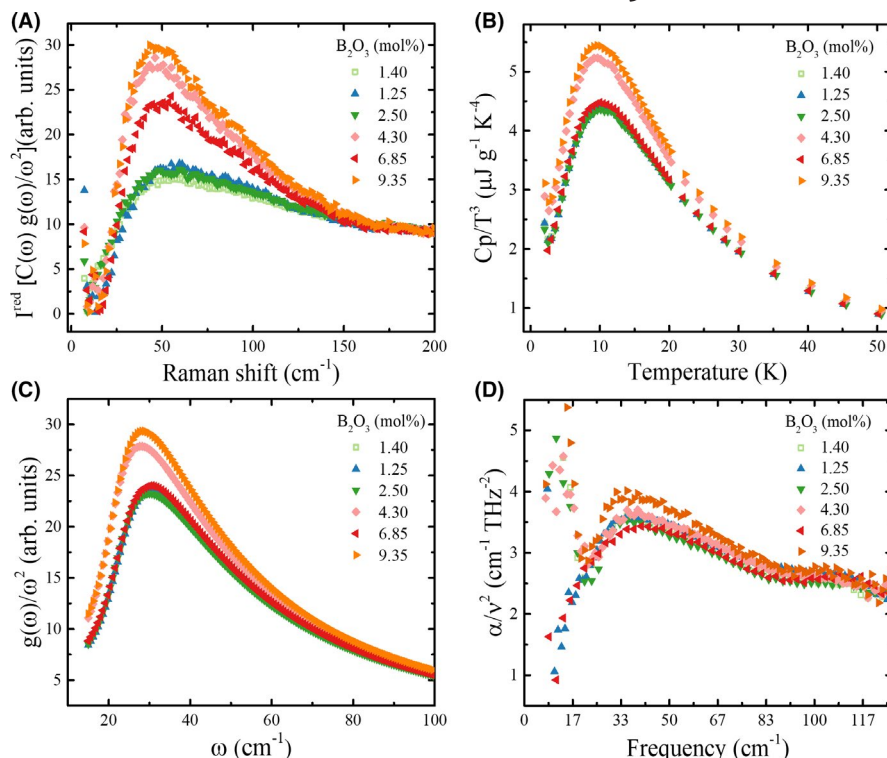


**FIGURE 3** Value of  $\omega_{Bp}$  from  $I_{red}(\omega)$  (red diamonds), THz-TDS (blue triangles) and  $C_p$ -VDOS  $g(\omega)/\omega^2$  (green squares) for aluminoborosilicate glasses [Color figure can be viewed at wileyonlinelibrary.com]

that is, when  $\omega_{Bp}$  shifts to lower frequencies, the corresponding intensity increases.

## 4 | DISCUSSION

### 4.1 | Short-range structure and mixing of network forming species

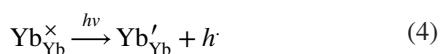
Several studies on the structure of high-silica borosilicate glasses agree that in the compositional range presently

investigated, the incorporation of boron oxide in the silica network occurs via the incorporation of trigonal  $[BO_3]$  units.<sup>51-53</sup> Furthermore, in alkali-containing glasses, the addition of  $Al_2O_3$  inhibits the formation of  $[BO_4^-]$  groups, as  $[AlO_4^-]$  are favored over  $[BO_4^-]$  groups for charge balancing,<sup>54-56</sup> resulting in a net conversion of tetrahedrally coordinated boron to trigonal, with aluminum being incorporated in the tetrahedral sites previously occupied by boron. This results in the formation of aluminum “bridges” -B-O-Al-O-Si- between the silicate and borate glass networks,<sup>9</sup> which is consistent with the common practice of adding small amounts of  $Al_2O_3$  to alkali-borosilicate glasses so as to avoid phase separation. NMR studies in aluminoborate glasses confirm that there is a strong preference for the formation of Al-O-B linkages.<sup>57-59</sup>

Regarding the present ternary glass series, the incorporation of boron oxide mainly as trigonal units is consistent with our mechanical characterization. The Poisson's ratio is a convenient probe of the overall network dimensionality,<sup>60</sup> and its observed increase with increasing  $B_2O_3$  concentration suggests a continuously decreasing dimensionality due to the addition of 2D triangular planar  $[BO_3]$  units in a fully polymerized  $[SiO_4]$  3D network. Interestingly, the atomic packing density of these glasses remains practically constant, implying that the decreasing mass density is a result of the substitution of  $[SiO_4]$  by lighter  $[BO_3]$  groups. The aforementioned homogenization in the distribution of plastic flow events (as signaled by the increasing strain-rate sensitivity) is also consistent with the decrease in intensity of the silica  $D_1$  and  $D_2$  defect bands. It seems likely that the addition of boron oxide preferentially breaks the highly strained 3- and 4-fold rings,

leading to the appearance of the broad feature centered at approximately  $690\text{ cm}^{-1}$  associated with the breathing modes of borosilicate rings. With regards to the boron connectivity, both Raman and IR spectra agree that for samples with less than 4.3 mol%  $\text{B}_2\text{O}_3$ , the  $[\text{BO}_3]$  groups seem to be present in silica or aluminosilicate environments. The appearance of the  $700\text{ cm}^{-1}$  feature for  $x \geq 6.85$  mol% indicates the formation of B-O-B bridges, and therefore more variability in the borate environment.

The first coordination shell of the ytterbium ions contains  $[\text{AlO}_4]$  (and  $[\text{SiO}_4]$ ) tetrahedra,<sup>28</sup> and the same aluminum environment is assumed to be the majority in our samples as it is consistent with literature reports on the coordination number of aluminum in high-silica glasses.<sup>29,61-66</sup> This coordination environment permits the occurrence of the reduction of  $\text{Yb}^{3+}$  to  $\text{Yb}^{2+}$  and the creation of a positively charged structural defect (Figures S1 and S2)<sup>67</sup>:



Here,  $h\nu$  represents the excitation energy for the charge transfer reaction. It corresponds to the formation of a transient positively charged hole,  $h$ , which is bound to the oxygen ligand. For aluminosilicate glasses doped with ytterbium ions, such defects were identified as Al-oxygen hole centers (OHC), formed by  $[\text{AlO}_4]^{\circ}$ .<sup>68</sup> In yttrium-doped aluminoborosilicates, the presence of oxygen triclusters coordinated by one RE ion and two four-coordinated trivalent species ( $\text{B}^{3+}$  and  $\text{Al}^{3+}$ ) seems to be energetically favorable.<sup>58</sup> In analogy, the positive hole created by the reduction of ytterbium when bound to an aluminum tetrahedron could take the role of a monovalent ion in the dynamic formation of the oxygen tricluster.<sup>69,70</sup> Such process could be responsible for the electrical conductivity results (Figure S3), where the conductivity of our samples is two orders of magnitude higher than that of fused silica,<sup>71,72</sup> and the estimated activation energies for DC conductivity are much lower than the reported values for diffusion of  $\text{Al}^{3+}$ ,  $\text{Yb}^{3+}$ ,  $\text{B}^{3+}$ ,  $\text{Si}^{4+}$  and  $\text{O}^{2-}$  in silicate glasses.<sup>28,73</sup> A combination of polaron hopping<sup>74,75</sup> between the ytterbium ions of different valence and the tricluster diffusion by bond switching<sup>69</sup> is hypothesized to be responsible for these results, as the impurity concentrations measured in our samples are too low to have such a strong effect.

## 4.2 | Boson peak position and scaling

From the position of the Raman Boson peak,  $\omega_{\text{BP}}$ , an empirical correlation length  $\xi$  associated with the size of the localized elastic heterogeneities in the glass matrix can be extracted,  $\xi = v_T/\omega_{\text{BP}}$ .<sup>76-78</sup> For the investigated aluminoborosilicate glasses, the correlation length increases monotonically with increasing  $\text{B}_2\text{O}_3$  concentration up to 4.3 mol%, whereas it strongly decreases for higher substitution levels (Figure 4).

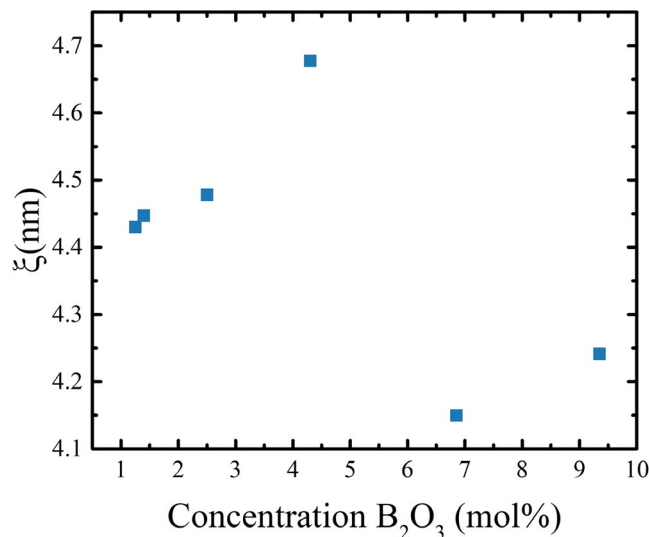


FIGURE 4 Empirical correlation length  $\xi$  in SAB:Yb glasses [Color figure can be viewed at wileyonlinelibrary.com]

Such a nonlinear compositional dependence indicates that there are major changes occurring in the short and intermediate range order. The correlation length is expected to be larger for more open structures and smaller in more densely packed ones.<sup>76</sup> For example, in binary sodium borates,  $\xi$  was found to be strongly correlated with the size of the superstructural units present in the glass.<sup>79</sup> The discontinuity shown in Figure 4 is consistent with our other results, where the measured properties are usually divided into two compositional ranges: up to 4.3 mol%  $\text{B}_2\text{O}_3$ , and above this value. Interestingly, density, refractive index, the elastic moduli, and hardness data do not show this compositional dependence. As they represent the response of a very large number of atoms, their behavior is dominated by the disruption of the 3D silica network with the addition of  $\text{B}_2\text{O}_3$ . However, characterization techniques which are more sensitive to local environments show similar nonlinear trends, and always change in the same compositional range.

A natural explanation for such behavior is that the incorporation of  $\text{B}_2\text{O}_3$  in these glasses does not occur randomly. As already discussed, boron seems to preferentially disrupt the highly strained three and fourfold silica rings (as seen from the decrease in the  $D_1$  and  $D_2$  defect bands in the Raman spectra – Figure 1A), but they are a minor component of the glassy network, with estimated concentrations of 1% or less.<sup>43</sup> The results from strain-rate sensitivity and  $H_3/H$  indicate that the disruption of the silica network is favored at concentrations above 4.3 mol%, as the distribution of plastic events in the network is homogenized and the overall bond dissociation energy starts to change.<sup>40</sup> This threshold is also consistent with the marked increase in the intensity of the IR band at  $1385\text{ cm}^{-1}$  for  $\text{B}_2\text{O}_3$  concentrations of 6.85 and 9.35 mol%, which is assigned to the vibrations of isolated  $[\text{BO}_3]$  triangles. Finally, the only

other possible site that could be preferentially attacked by boron are the Al-O-Si bridges, which is consistent with our observations from UV-Vis, photoluminescence, and electrochemical impedance (see Supplementary Information) as they suggest a higher concentration of the ytterbium-centered defects (and possibly of oxygen triclusters) for compositions with lower amounts of B<sub>2</sub>O<sub>3</sub>. This high defect concentration is then reflected on the compositional dependence of the activation energy for conductivity as the presence of boron and aluminum around a reduced ytterbium ion is necessary to stabilize the thus-created structural defects.

Substitution of SiO<sub>2</sub> by B<sub>2</sub>O<sub>3</sub> compensates for the basic contribution of Al<sub>2</sub>O<sub>3</sub> which enhanced the electron donor capability in SiO<sub>2</sub>-Al<sub>2</sub>O<sub>3</sub> networks (with B<sub>2</sub>O<sub>3</sub> adding a more acidic character relative to SiO<sub>2</sub> or Al<sub>2</sub>O<sub>3</sub>). For a molar content of ~1.5% of Al<sub>2</sub>O<sub>3</sub>, the basicity of pure

SiO<sub>2</sub> is recovered by substituting ~3.5-4.5 mol% of SiO<sub>2</sub> by B<sub>2</sub>O<sub>3</sub> (see Figure S3). From this chemical viewpoint, such a substitution ratio could therefore represent the most stable (best-mixed) state.

In order to investigate the frequency of the Boson peak with changes in the elastic medium transformation, a Debye corrected representation for Bp-VDOS is investigated by evaluating the Debye frequency  $\omega_D$  and Debye DOS  $g_D(\omega)$  in terms of longitudinal and transverse sound velocities<sup>80</sup>

$$\omega_D = k_D \left[ \frac{1}{3} \left( \frac{1}{v_L^3} + \frac{2}{v_T^3} \right) \right]^{-1/3} \quad (5)$$

$$g_D(\omega) = 3\omega^3/\omega_D^3 \quad (6)$$

Normalizing the frequency by  $\omega/\omega_D$  and the DoS by  $g(\omega)/g_D(\omega)$  reveals how variations in external parameters such as temperature, pressure or the amount of polarization fall within the regime of continuous elastic medium transformations.<sup>81</sup> In terms of the CPA model, if disorder does not change but just the value of the mean elastic constants or density, all data points should fall onto a single master curve. In the present investigations (Figure 5), this is clearly not the case because the addition of B<sub>2</sub>O<sub>3</sub> modifies the glass structure and, consequently, the state of disorder is changed by changing the external conditions.<sup>81</sup>

For a substitution ratio of  $1.7 < B/Al < 2.7$  (~2 by interpolation, see Figure S3), the electron donor capability of the basic Al (and Yb) component is compensated by the more acidic B species. This reflects in a minimum in electrical conductivity (Figure S4) and a theoretical optical basicity which approaches the one of a pure silica glass. In Figure 6, the three corresponding structural regimes are depicted schematically: (a) aluminum-sites containing one or two boron atoms in the second shell for  $B/Al < 2$ ; (b) aluminum-sites saturated with three boron atoms in the second shell for  $B/Al \sim 2-3$  and; (c) aluminum-sites with

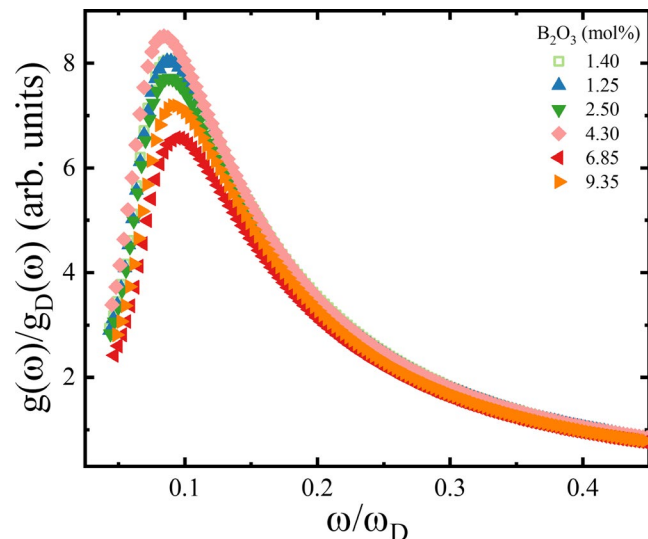


FIGURE 5 Reduced vibrational density of states  $g(\omega)/g_D(\omega)$  vs. the rescaled frequency  $\omega/\omega_D$  [Color figure can be viewed at wileyonlinelibrary.com]

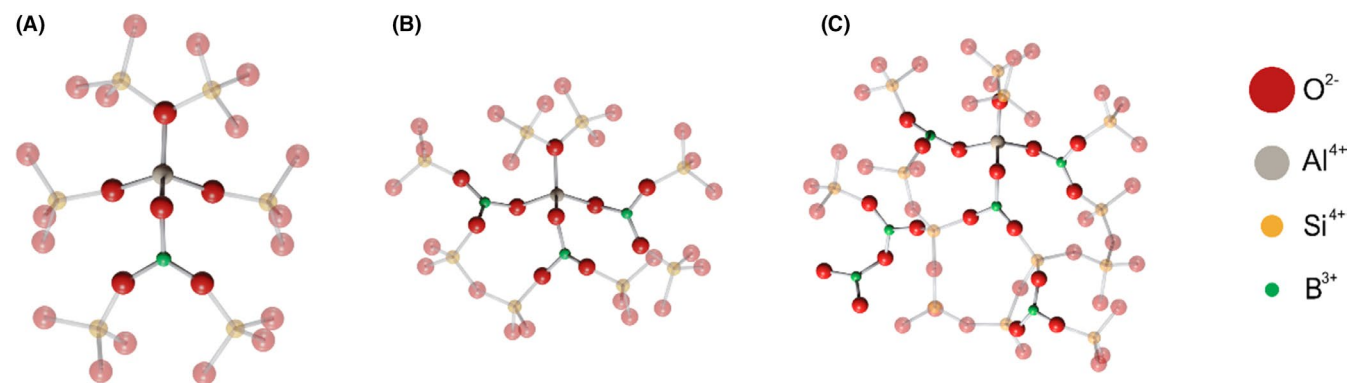


FIGURE 6 Schematic representation of aluminum sites in ternary aluminoborosilicate glasses based on NMR investigations<sup>57,58,82</sup> (see text for details). (A) aluminum sites for  $B/Al$  ratio  $\leq 2$ , (B) for  $B/Al$  ratio  $\sim 2-3$  and, (C) for  $B/Al$  ratio  $> 3$  [Color figure can be viewed at wileyonlinelibrary.com]

three boron atoms in the second shell and a silica network containing Si/B-O-B/Si bonds for B/Al > 3. Excepting the sample with elevated Yb<sup>2+</sup> content (1.4 mo% B<sub>2</sub>O<sub>3</sub>), the highest PL emission intensity was found for the samples with B/Al ~2-3, indicating a possible shielding effect of B in these concentrations. The observations on intermediate length scales, as probed by the boson peak measurements, corroborate these interpretations.

## 5 | CONCLUSIONS


We considered the low-frequency vibrational modes of aluminoborosilicate glasses as a means to assess material heterogeneity on an intermediate length scale. Using low-temperature heat capacity, low-frequency Raman scattering data and THz-TDS, we scaled the vibrational density of states and the Boson peak. Across the studied range of B<sub>2</sub>O<sub>3</sub>-for-SiO<sub>2</sub> substitution, we find a characteristic regime in which the Boson peak position and the extracted correlation length exhibit a marked discontinuity. This discontinuity reappears in the macroscopic electrical conductivity, and also in the strain rate sensitivity of material hardness. The characteristic composition coincides with the theoretical acidity of a pure silica glass, whereby the electron donor capability of Al<sub>2</sub>O<sub>3</sub> (and Yb<sub>2</sub>O<sub>3</sub>) is compensated by the more acidic B<sub>2</sub>O<sub>3</sub>. This constitutes an optimal value for the ratio of B/(Al+Yb) in terms of mixture stability. Al<sub>2</sub>O<sub>3</sub> plays a mediating role in the structure of aluminoborosilicate glasses, facilitating homogeneity of the SiO<sub>2</sub> - B<sub>2</sub>O<sub>3</sub> mixed network and dissolution of Yb<sub>2</sub>O<sub>3</sub> into the silica backbone.

## ACKNOWLEDGMENTS

This project has received funding from the European Research Council (ERC) under the European Union's Horizon 2020 research and innovation program (L.W., ERC grant UTOPEs, grant agreement no. 681652), and from the Carl Zeiss Foundation within its Research Infrastructures program. We thank our colleagues at OSIM and IPHT for valuable support with sample preparation and physical data acquisition.

## ORCID

Tatsuya Mori  <https://orcid.org/0000-0002-9443-594X>

Stefan G. Ebbinghaus  <https://orcid.org/0000-0001-6391-2582>

Lothar Wondraczek  <https://orcid.org/0000-0002-0747-3076>

## REFERENCES

- Ando MF, Benzine O, Pan Z, Garden J-L, Wondraczek K, Grimm S, et al. Boson peak, heterogeneity and intermediate-range order in binary SiO<sub>2</sub>-Al<sub>2</sub>O<sub>3</sub> glasses. *Sci Rep.* 2018;8(1):5394. <https://doi.org/10.1038/s41598-018-23574-1>
- Potuzak M, Smedskjaer MM. Physical properties of boroaluminosilicate glasses: effect of modifier cation field strength. *Phys Chem Glas - Eur J Glas Sci and Technology Part B.* 2014;55(1):18–24.
- Du L-S, Stebbins JF. Network connectivity in aluminoborosilicate glasses: a high-resolution <sup>11</sup>B, <sup>27</sup>Al and <sup>17</sup>O NMR study. *J Non Cryst Solids.* 2005;351(43):3508–20. <https://doi.org/10.1016/j.jnoncrysol.2005.08.033>
- Kidari A, Magnin M, Caraballo R, Tribet M, Doreau F, Peugot S, et al. Solubility and partitioning of minor-actinides and lanthanides in aluminoborosilicate nuclear glass. *Procedia Chem.* 2012;7:554–8. <https://doi.org/10.1016/j.proche.2012.10.084>
- Van Uitert LG, Pinnow DA, Williams JC, Rich TC, Jaeger RE, Grodkiewicz WH. Borosilicate glasses for fiber optical waveguides. *Mater Res Bull.* 1973;8(4):469–76. [https://doi.org/10.1016/0025-5408\(73\)90051-2](https://doi.org/10.1016/0025-5408(73)90051-2)
- Wu J, Stebbins JF. Quench rate and temperature effects on boron coordination in aluminoborosilicate melts. *J Non Cryst Solids.* 2010;356(41):2097–108. <https://doi.org/10.1016/j.jnoncrysol.2010.08.015>
- Wu J, Potuzak M, Stebbins JF. High-temperature in situ <sup>11</sup>B NMR study of network dynamics in boron-containing glass-forming liquids. *J Non Cryst Solids.* 2011;357(24):3944–51. <https://doi.org/10.1016/j.jnoncrysol.2011.08.013>
- Stebbins JF, Wu J, Thompson LM. Interactions between network cation coordination and non-bridging oxygen abundance in oxide glasses and melts: Insights from NMR spectroscopy. *Chem Geol.* 2013;346:34–46. <https://doi.org/10.1016/j.chemgeo.2012.09.021>
- Du W-F, Kuraoka K, Akai T, Yazawa T. Study of Al<sub>2</sub>O<sub>3</sub> effect on structural change and phase separation in Na<sub>2</sub>O-B<sub>2</sub>O<sub>3</sub>-SiO<sub>2</sub> glass by NMR. *J Mater Sci.* 2000;35(19):4865–71. <https://doi.org/10.1023/a:1004853603298>
- Du L-S, Stebbins JF. Site connectivities in sodium aluminoborate glasses: multinuclear and multiple quantum NMR results. *Solid State Nucl Magn Reson.* 2005;27(1):37–49. <https://doi.org/10.1016/j.ssnmr.2004.08.003>
- Calas G, Cormier L, Galois L, Jollivet P. Structure-property relationships in multicomponent oxide glasses. *Comptes Rendus Chim.* 2002;5:831–43. [https://doi.org/10.1016/S1631-0748\(02\)01459-5](https://doi.org/10.1016/S1631-0748(02)01459-5)
- Vacher R, Rufflé B, Hehlen B, Guimbrètière G, Simon G, Courtens E. The vibrational excitations of glasses in the boson-peak region: application to borates. *Phys Chem Glas - Eur J Glas Sci and Technology Part B.* 2008;49(1):19–25.
- Zhang L, Zheng J, Wang Y, Zhang L, Jin Z, Hong L, et al. Experimental studies of vibrational modes in a two-dimensional amorphous solid. *Nat Commun.* 2017;8(1):67. <https://doi.org/10.1038/s41467-017-00106-5>
- Elliott SR. *Physics of amorphous materials.* London, New York: Longman Group Ltd.; 1984.
- Greaves GN, Meneau F, Majerus O, Jones DG, Taylor J. Identifying vibrations that destabilize crystals and characterize the glassy state. *Science.* 2005;308(5726):1299–302. <https://doi.org/10.1126/science.1109411>
- Chumakov AI, Monaco G, Monaco A, et al. Equivalence of the boson peak in glasses to the transverse acoustic van Hove singularity in crystals. *Phys Rev Lett.* 2011;106(22):225501. <https://doi.org/10.1103/PhysRevLett.106.225501>
- Schirmacher W, Ruocco G. Heterogeneous elasticity: the tale of the boson peak. *arXiv:200905970v1.* n.d.
- Thorpe MF, Tichý L. *Properties and applications of amorphous materials.* Springer Science & Business Media; 2012.



19. Kabeya M, Mori T, Fujii Y, Koreeda A, Lee BW, Ko J-H, et al. Boson peak dynamics of glassy glucose studied by integrated terahertz-band spectroscopy. *Phys Rev B*. 2016;94(22):224204. <https://doi.org/10.1103/PhysRevB.94.224204>
20. Caponi S, Corezzi S, Fioretto D, Fontana A, Monaco G, Rossi F. Raman-scattering measurements of the vibrational density of states of a reactive mixture during polymerization: effect on the boson peak. *Phys Rev Lett*. 2009;102(2):27402.
21. Marruzzo A, Schirmacher W, Fratallocchi A, Ruocco G. Heterogeneous shear elasticity of glasses: the origin of the boson peak. *Sci Rep*. 2013;3:1407. <https://doi.org/10.1038/srep01407>
22. Benzine O, Bruns S, Pan Z, Durst K, Wondraczek L. Local deformation of glasses is mediated by rigidity fluctuation on nanometer scale. *Adv Sci*. 2018;5(10):1800916. <https://doi.org/10.1002/advs.201800916>
23. Schuster K, Grimm S, Kalide A, Dellith J, Leich M, Schwuchow A, et al. Evolution of fluorine doping following the REPUSIL process for the adjustment of optical properties of silica materials. *Opt Mater Express*. 2015;5(4):887–97. <https://doi.org/10.1364/OME.5.000887>
24. Schuster K, Unger S, Aichele C, Lindner F, Grimm S, Litzkendorf D, et al. Material and technology trends in fiber optics. *Adv Opt Technol*. 2014;3(4). <https://doi.org/10.1515/aot-2014-0010>
25. Langner A, Schötz G, Such M, et al. A new material for high-power laser fibers. *Lasers Appl Sci Eng*. 2008;6873:687311–9.
26. Wang J. Alumina as a dopant in optical fiber by OVD. *Appl Phys A*. 2014;116(2):505–18. <https://doi.org/10.1007/s00339-014-8525-x>
27. Deschamps T, Ollier N, Vezin H, Gonnet C. Clusters dissolution of Yb<sup>3+</sup> in codoped SiO<sub>2</sub>-Al<sub>2</sub>O<sub>3</sub>-P<sub>2</sub>O<sub>5</sub> glass fiber and its relevance to photodarkening. *J Chem Phys*. 2012;136(1):14503. <https://doi.org/10.1063/1.3673792>
28. Unger S, Dellith J, Scheffel A, Kirchhof J. Diffusion in Yb<sub>2</sub>O<sub>3</sub>-Al<sub>2</sub>O<sub>3</sub>-SiO<sub>2</sub> glass. *Phys Chem Glas J Glas Sci Technol Part B*. 2011;52(2):41–6.
29. Sen S. Atomic environment of high-field strength Nd and Al cations as dopants and major components in silicate glasses: a Nd LIII-edge and Al K-edge X-ray absorption spectroscopic study. *J Non Cryst Solids*. 2000;261(1):226–36. [https://doi.org/10.1016/S0022-3093\(99\)00564-5](https://doi.org/10.1016/S0022-3093(99)00564-5)
30. Lægsgaard J. Dissolution of rare-earth clusters in SiO<sub>2</sub> by Al codoping: a microscopic model. *Phys Rev B*. 2002;65(17):174114. <https://doi.org/10.1103/PhysRevB.65.174114>
31. Limbach R, Rodrigues BP, Möncke D, Wondraczek L. Elasticity, deformation and fracture of mixed fluoride-phosphate glasses. *J Non Cryst Solids*. 2015;430:99–107. <https://doi.org/10.1016/j.jnoncrysol.2015.09.025>
32. Limbach R, Winterstein-Beckmann A, Dellith J, Möncke D, Wondraczek L. Plasticity, crack initiation and defect resistance in alkali-borosilicate glasses: from normal to anomalous behavior. *J Non Cryst Solids*. 2015;417–418:15–27. <https://doi.org/10.1016/j.jnoncrysol.2015.02.019>
33. Limbach R, Karlsson S, Scannell G, Mathew R, Edén M, Wondraczek L. The effect of TiO<sub>2</sub> on the structure of Na<sub>2</sub>O-CaO-SiO<sub>2</sub> glasses and its implications for thermal and mechanical properties. *J Non Cryst Solids*. 2017;471:6–18. <https://doi.org/10.1016/j.jnoncrysol.2017.04.013>
34. Limbach R, Rodrigues BP, Wondraczek L. Strain-rate sensitivity of glasses. *J Non Cryst Solids*. 2014;404:124–34. <https://doi.org/10.1016/j.jnoncrysol.2014.08.023>
35. Sawamura S, Limbach R, Behrens H, Wondraczek L. Lateral deformation and defect resistance of compacted silica glass: quantification of the scratching hardness of brittle glasses. *J Non Cryst Solids*. 2018;481:503–11. <https://doi.org/10.1016/j.jnoncrysol.2017.11.035>
36. Shuker R, Gammon RW. Raman-scattering selection-rule breaking and the density of states in amorphous materials. *Phys Rev Lett*. 1970;25(4):222–5.
37. Köhler S, Ruocco G, Schirmacher W. Coherent potential approximation for diffusion and wave propagation in topologically disordered systems. *Phys Rev B*. 2013;88(6):64203.
38. Schirmacher W, Diezemann G, Ganter C. Harmonic vibrational excitations in disordered solids and the “boson peak”. *Phys Rev Lett*. 1998;81(1):136–9. <https://doi.org/10.1103/PhysRevLett.81.136>
39. Schirmacher W, Ruocco G, Mazzone V. Heterogeneous viscoelasticity: a combined theory of dynamic and elastic heterogeneity. *Phys Rev Lett*. 2015;115(1):15901.
40. Sawamura S, Wondraczek L. Scratch hardness of glass. *Phys Rev Mater*. 2018;2(9):092601. <https://doi.org/10.1103/PhysRevMaterials.2.092601>
41. Rodrigues BP, Limbach R, de Souza GB, Ebendorff-Heidepriem H, Wondraczek L. Correlation between ionic mobility and plastic flow events in NaPO<sub>3</sub>-NaCl-Na<sub>2</sub>SO<sub>4</sub> glasses. *Front Mater*. 2019;6:1–13. <https://doi.org/10.3389/fmats.2019.00128>
42. Limbach R, Kosiba K, Pauly S, Kuhn U, Wondraczek L. Serrated flow of CuZr-based bulk metallic glasses probed by nanoindentation: role of the activation barrier, size and distribution of shear transformation zones. *J Non Cryst Solids*. 2017;459:130–41. <https://doi.org/10.1016/j.jnoncrysol.2017.01.015>
43. Galeener FL. Planar rings in glasses. *Solid State Commun*. 1982;44(7):1037–40. [https://doi.org/10.1016/0038-1098\(82\)90329-5](https://doi.org/10.1016/0038-1098(82)90329-5)
44. Konijnendijk WL, Stevels JM. The structure of borosilicate glasses studied by Raman scattering. *J Non Cryst Solids*. 1976;20:193–224. [https://doi.org/10.1016/0022-3093\(76\)90132-0](https://doi.org/10.1016/0022-3093(76)90132-0)
45. Furukawa T, White WB. Raman spectroscopic investigation of sodium borosilicate glass structure. *J Mater Sci*. 1981;16(10):2689–700. <https://doi.org/10.1007/bf00552951>
46. Yadav AK, Singh P. A review of the structures of oxide glasses by Raman spectroscopy. *RSC Adv*. 2015;5:67583–609. <https://doi.org/10.1039/c5ra13043c>
47. Manara D, Grandjean A, Neuville DR. Advances in understanding the structure of borosilicate glasses: a Raman spectroscopy study. *Am Mineral*. 2009;94:777–84. <https://doi.org/10.2138/am.2009.3027>
48. Kirk CT. Quantitative analysis of the effect of disorder-induced mode coupling on infrared absorption in silica. *Phys Rev B*. 1988;38(2):1255–73.
49. Shibata N, Horigudhi M, Edahiro T. Raman spectra of binary high-silica glasses and fibers containing GeO<sub>2</sub>, P<sub>2</sub>O<sub>5</sub> and B<sub>2</sub>O<sub>3</sub>. *J Non Cryst Solids*. 1981;45(1):115–26. [https://doi.org/10.1016/0022-3093\(81\)90096-X](https://doi.org/10.1016/0022-3093(81)90096-X)
50. Tenney AS, Wong J. Vibrational spectra of vapor-deposited binary borosilicate glasses. *J Chem Phys*. 1972;56(11):5516–23. <https://doi.org/10.1063/1.1677069>
51. Martens R, Müller-Warmuth W. Structural groups and their mixing in borosilicate glasses of various compositions – an NMR study. *J Non Cryst Solids*. 2000;265(1–2):167–75. [https://doi.org/10.1016/S0022-3093\(99\)00693-6](https://doi.org/10.1016/S0022-3093(99)00693-6)
52. Wang S, Stebbins JF. Multiple-quantum magic-angle spinning 17O NMR studies of borate, borosilicate, and borosilicate glasses.

- J Am Ceram Soc. 2004;82(6):1519–28. <https://doi.org/10.1111/j.1151-2916.1999.tb01950.x>
53. Soleilhavoup A, Delage J-M, Angeli F, Caurant D, Charpentier T. Contribution of first-principles calculations to multinuclear NMR analysis of borosilicate glasses. *Magn Reson Chem*. 2010;48(S1):S159–S170. <https://doi.org/10.1002/mrc.2673>
  54. Wu J, Stebbins JF. Effects of cation field strength on the structure of aluminoborosilicate glasses: high-resolution  $^{11}\text{B}$ ,  $^{27}\text{Al}$  and  $^{23}\text{Na}$  MAS NMR. *J Non Cryst Solids*. 2009;355(9):556–62. <https://doi.org/10.1016/j.jnoncrsol.2009.01.025>
  55. Zheng Q, Potuzak M, Mauro JC, Smedskjaer MM, Youngman RE, Yue Y. Composition–structure–property relationships in boroaluminosilicate glasses. *J Non Cryst Solids*. 2012;358(6–7):993–1002. <https://doi.org/10.1016/j.jnoncrsol.2012.01.030>
  56. Bruns S, Uesbeck T, Weil D, Möncke D, van Wüllen L, Durst K, et al. Influence of  $\text{Al}_2\text{O}_3$  addition on structure and mechanical properties of borosilicate glasses. *Front Mater*. 2020;7:189. <https://doi.org/10.3389/fmats.2020.00189>
  57. Bertmer M, Züchner L, Chan JCC, Eckert H. Short and medium range order in sodium aluminoborate glasses. 2. Site connectivities and cation distributions studied by rotational echo double resonance NMR spectroscopy. *J Phys Chem B*. 2000;104(28):6541–53. <https://doi.org/10.1021/jp9941918>
  58. Deters H, de Lima JF, Magon CJ, de Camargo ASS, Eckert H. Structural models for yttrium aluminium borate laser glasses: NMR and EPR studies of the system  $(\text{Y}_2\text{O}_3)_0.2 - (\text{Al}_2\text{O}_3)_x - (\text{B}_2\text{O}_3)_{0.8-x}$ . *Phys Chem Chem Phys*. 2011;13(35):16071–83. <https://doi.org/10.1039/C1CP21404G>
  59. Cheng Y, Xiao H, Shuguang C, Tang B. Structure and crystallization of  $\text{B}_2\text{O}_3\text{-Al}_2\text{O}_3\text{-SiO}_2$  glasses. *Phys B Condens Matter*. 2009;404(8–11):1230–4. <https://doi.org/10.1016/j.physb.2008.11.198>
  60. Greaves GN, Greer AL, Lakes RS, Rouxel T. Poisson's ratio and modern materials. *Nat Mater*. 2011;10:823–37. <https://doi.org/10.1038/nmat3134>
  61. Pfleiderer P, Horbach J, Binder K. Structure and transport properties of amorphous aluminium silicates: computer simulation studies. *Chem Geol*. 2006;229(1–3):186–97. <https://doi.org/10.1016/j.chemgeo.2006.01.020>
  62. Schmücker M, MacKenzie KD, Schneider H, Meinhold R. NMR studies on rapidly solidified  $\text{SiO}_2\text{-Al}_2\text{O}_3$  and  $\text{SiO}_2\text{-Al}_2\text{O}_3\text{-Na}_2\text{O}$  glasses. *J Non Cryst Solids*. 1997;217(1):99–105. [https://doi.org/10.1016/S0022-3093\(97\)00127-0](https://doi.org/10.1016/S0022-3093(97)00127-0)
  63. Hanada T, Bessyo Y, Soga N. Elastic constants of amorphous thin films in the systems  $\text{SiO}_2\text{-Al}_2\text{O}_3$  and  $\text{AlPO}_4\text{-Al}_2\text{O}_3$ . *J Non Cryst Solids*. 1989;113(2–3):213–20. [https://doi.org/10.1016/0022-3093\(89\)90014-8](https://doi.org/10.1016/0022-3093(89)90014-8)
  64. Sen S, Youngman RE. High-resolution multinuclear NMR structural study of binary aluminosilicate and other related glasses. *J Phys Chem B*. 2004;108(23):7557–64. <https://doi.org/10.1021/jp031348u>
  65. Fukumi K, Chayahara A, Kitamura N, Nishii J, Kadono K, Makihara M, et al. Refractive index change in  $\text{Al}^{3+}$ -ion-implanted silica glass. *J Appl Phys*. 1996;79(2):1060. <https://doi.org/10.1063/1.360894>
  66. Guo M, Shao C, Zhang Y, et al. Effect of  $\text{B}_2\text{O}_3$  addition on structure and properties of  $\text{Yb}^{3+}/\text{Al}^{3+}/\text{B}^{3+}$ -co-doped silica glasses. *J Am Ceram Soc*. 2020;103(8):4275–85. <https://doi.org/10.1111/jace.17155>
  67. Rydberg S, Engholm M. Experimental evidence for the formation of divalent ytterbium in the photodarkening process of Yb-doped fiber lasers. *Opt Express*. 2013;21(6):6681–8. <https://doi.org/10.1364/OE.21.006681>
  68. Arai T, Ichii K, Okada K, Kitabayashi T, Tanigawa S, Fujimaki M. Photodarkening phenomenon in Yb-doped fibers. *Fujikura Giho*. 2008;6–11.
  69. Toplis MJ, Dingwell DB, Lenci T. Peraluminous viscosity maxima in  $\text{Na}_2\text{O-Al}_2\text{O}_3\text{-SiO}_2$  liquids: the role of triclusters in tectosilicate melts. *Geochim Cosmochim Acta*. 1997;61(13):2605–12.
  70. Kubicki JD, Toplis MJ. Molecular orbital calculations on aluminosilicate tricluster molecules: Implications for the structure of aluminosilicate glasses. *Am Mineral*. 2002;87(5–6):668–78. <https://doi.org/10.2138/am-2002-5-609>
  71. Strauss SW. Electrical resistivity of vitreous ternary lithium-sodium silicates. *J Res Natl Bur Stand*. 1956;56(4):183. <https://doi.org/10.6028/jres.056.025>
  72. Brückner R. Properties and structure of vitreous silica. II. *J Non Cryst Solids*. 1971;5(3):177–216. [https://doi.org/10.1016/0022-3093\(71\)90032-9](https://doi.org/10.1016/0022-3093(71)90032-9)
  73. Nasciment MLF, Zanotto ED. Diffusion processes in vitreous silica revisited. *Phys Chem Glas - Eur J Glas Sci Technol Part B*. 2007;48(4):201–17.
  74. Cramer C, Funke K, Roling B, Saatkamp T, Wilmer D, Ingram MD, et al. Ionic and polaronic hopping in glass. *Solid State Ionics*. 1996;86–88:481–6. [https://doi.org/10.1016/0167-2738\(96\)00178-6](https://doi.org/10.1016/0167-2738(96)00178-6)
  75. Al-Shahrani A, Al-Hajry A, El-Desoky MM. Non-adiabatic small polaron hopping conduction in sodium borate tungstate glasses. *Phys Status Solidi*. 2003;200(2):378–87. <https://doi.org/10.1002/pssa.200306689>
  76. Elliott SR. A unified model for the low-energy vibrational behaviour of amorphous solids. *Europhys Lett*. 1992;19(3):201–6. <https://doi.org/10.1209/0295-5075/19/3/009>
  77. Duval E, Boukenter A, Achibat T. Vibrational dynamics and the structure of glasses. *J Phys Condens Matter*. 1990;2(51):10227.
  78. Duval E, Mermet A, Saviot L. Boson peak and hybridization of acoustic modes with vibrations of nanometric heterogeneities in glasses. *Phys Rev B*. 2007;75(2):24201.
  79. Osipov AA, Osipova LM. Boson peak and superstructural groups in  $\text{Na}_2\text{O-B}_2\text{O}_3$  glasses. *Adv Condens Matter Phys*. 2018;6746023. <https://doi.org/10.1155/2018/6746023>
  80. Schirmacher W, Ruocco G, Scopigno T. Acoustic attenuation in glasses and its relation with the boson peak. *Phys Rev Lett*. 2007;98(2):25501. <https://doi.org/10.1103/PhysRevLett.98.025501>
  81. Schirmacher W, Scopigno T, Ruocco G. Theory of vibrational anomalies in glasses. *J Non Cryst Solids*. 2015;407:133–40. <https://doi.org/10.1016/j.jnoncrsol.2014.09.054>
  82. Deters H, de Camargo ASS, Santos CN, Ferrari CR, Hernandez AC, Ibanez A, et al. Structural characterization of rare-earth doped yttrium aluminoborate laser glasses using solid state NMR. *J Phys Chem C*. 2009;113(36):16216–25. <https://doi.org/10.1021/jp9032904>

## SUPPORTING INFORMATION

Additional supporting information may be found online in the Supporting Information section.

**How to cite this article:** Ando MF, Fuhrmann S, Pan Z, et al. Boson peak and structural heterogeneity in ternary  $\text{SiO}_2\text{-Al}_2\text{O}_3\text{-B}_2\text{O}_3$  glasses. *J Am Ceram Soc*. 2021;104:4991–5000. <https://doi.org/10.1111/jace.17771>